Carbohydrate Polymers 87 (2012) 644–649

Contents lists available at SciVerse ScienceDirect

Carbohydrate Polymers

journal homepage: www.elsevier.com/locate/carbpol

A mechanically strong, flexible and conductive film based on bacterial cellulose/graphene nanocomposite

Yiyu Feng[a,b], Xuequan Zhang[a,b], Yongtao Shen[a,b], Katsumi Yoshino[c], Wei Feng[a,b,*]

[a] School of Materials Science and Engineering, Tianjin University, Tianjin 300072, PR China
[b] Tianjin Key Laboratory of Composite and Functional Materials, Tianjin 300072, PR China
[c] Shimane Institute for Industrial Technology, Hokuryo-cho, Matsue, Shimane 690-0816, Japan

ARTICLE INFO

Article history:
Received 29 April 2011
Received in revised form 7 July 2011
Accepted 16 August 2011
Available online 22 August 2011

Keywords:
Bacterial cellulose
Graphene oxide
Flexible
Conductivity

ABSTRACT

A highly flexible nanocomposite film of bacterial cellulose (BC) and graphene oxide (GO) with a layered structure was presented using the vacuum-assisted self-assembly technique. Microscopic and X-ray diffraction measurements demonstrated that the GO nanosheets were uniformly dispersed in the BC matrix. The interactions between BC and GO were studied by Fourier transformation infrared spectroscopy. Compared with pristine BC, the integration of 5 wt% GO resulted in 10% and 20% increase in Young's modulus and tensile strength of the composite film. The electrical conductivity of the composite film containing 1 wt% GO after in situ reduction showed a remarkable increase by 6 orders of magnitude compared with the insulated BC.

1. Introduction

Functional nanocomposites or nanohybrids based on biopolymers and nanometer-scale fillers are of scientific and industrial interest for their biofunctionality and notable performance improvement (Sellinger et al., 1998). As a natural polymer, bacterial cellulose (BC) has garnered considerable attention on account of its high tensile strength and crystallinity, good water-holding capacity, and biocompatibility (Czaja, Young, Kawecki, & Brown, 2007; Klemm, Schumann, Udhardt, & Marsch, 2001; Klemm, Heublein, Fink, & Bohn, 2005). It has found a multitude of applications in the paper and food industries, sewage purification, and composite reinforcement (El-Saied, Basta, & Gobran, 2004; Nakagaito, Iwamoto, & Yano, 2005; Vandamme, De Baets, Vanbaelen, Joris, & De Wulf, 1998). For the last application, various efforts have been made to maximize the benefits of nanocomposites based on BC through the combination of other materials (Yang et al., 2009; Yano et al., 2005) or the modified cellulose biosynthesis (Park, Kim, Kwon, Hong, & Jin, 2009; Yan et al., 2008). Among several methods, the integration of unique carbon nanomaterials into the BC matrix is regarded as one of ideal building blocks for the improvement of the mechanical and electrical properties. As a one-dimensional nanomaterial with high aspect ratio, carbon nanotube (CNT) has been incorporated into the BC matrix, showing enhanced mechanical strength and electrical conductivity (Chen, Kim, Kwon, Yun, & Jin, 2009; Yoon, Jin, Kook, & Pyun, 2006). Yoon et al. (2006) prepared BC/CNT nanocomposite by dipping the cellulose pellicles into a multi-walled carbon nanotube (MWCNT) solution. The conductivity of the BC pellicle with 9.6 wt% of MWCNTs reached 1.4×10^{-1} S/cm.

Graphene, a two-dimensional sheet of sp^2-hybridized carbon arranged in a hexagonal lattice, has revealed a variety of mechanical and electrical properties that qualify it for the reinforcement of polymer matrixes. Recently, much work has been targeted on mechanically or electrically enhanced polymers using the nanosheets of graphene oxide (GO) or reduced graphene oxide (RGO) as nanofillers (Salavagione, Gomez, & Martinez, 2009; Steurer, Wissert, Thomann, & Mulhaupt, 2009; Wu & Liu, 2010; Xu, Wang, Zu, Han, & Wei, 2010). Results showed that uniform dispersion of graphene in the polymer matrix was necessary in order to obtain the best characteristics. Specifically, GO shows the strong functionalities and processibilities due to the oxygen-containing functional groups on its basal planes and edges (Kovtyukhova et al., 1999; Stankovich, Piner, Nguyen, & Ruoff, 2006). Moreover, BC is water soluble in NaOH solution at a relative low temperature (Isogai & Atalla, 1998). Thus, BC/GO nanocomposite films can be easily obtained by filtering a colloidal solution of GO that has been pre-dispersed in the BC aqueous solution through a simple vacuum-assistant self-assembly method. It is noteworthy that the functionality of the nanocomposite not only depends on the natural property of each component, but also is closely related to the synergistic effect between them. Because of the many hydroxyl groups

* Corresponding author at: Tianjin University, School of Materials Science and Engineering, Tianjin 300072, PR China. Fax: +86 22 87402059.
E-mail address: weifeng@tju.edu.cn (W. Feng).

0144-8617/$ – see front matter © 2011 Elsevier Ltd. All rights reserved.
doi:10.1016/j.carbpol.2011.08.039

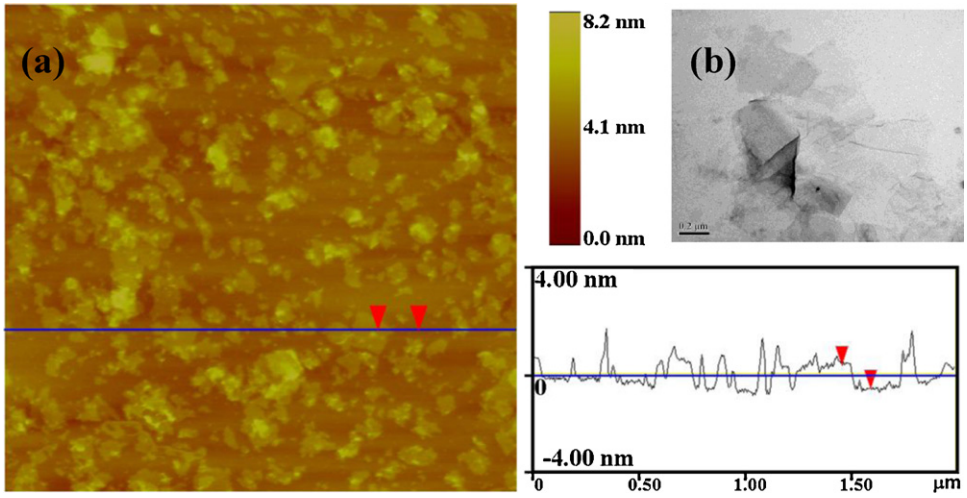

Fig. 1. GO sheets shown by (a) AFM with a 2 μm scale and the corresponding height profile and (b) TEM showing inclusions of GO sheets, scale bar = 0.2 μm.

in the BC units, effective interactions between BC and GO such as electrostatic interaction and hydrogen bonding are potentially achievable, which are important for the mechanical enhancements of the composite film.

Herein we presented a mechanically strong, flexible and conductive film based on BC/GO nanocomposite with the assistance of a vacuum. The dispersion of GO in the BC matrix was investigated by scanning electron microscopy (SEM). Fourier transformation infrared (FT-IR) spectra indicated the hydrogen bonding interaction between BC and GO. The integration of GO disrupted the aggregation and crystallinity of the BC matrix. Enhanced mechanical strength of the BC/GO nanocomposite films were observed compared with that of pristine BC. After in situ reduction, the BC/RGO films showed a notable improvement in electrical conductivity.

2. Experimental

2.1. Materials

GO was produced by the modified Hummers method through the acid oxidation of flake graphite (Becerril, Mao, Liu, Stoltenberg, Bao, & Chen, 2008; Hummers & Offeman, 1958). BC was supported by Space Environmental Technology Company, Limited, Japan. It was first washed with distilled water, followed by immersion in a 5 wt% NaOH solution for 15 h, and was finally re-washed with distilled water for 10 times.

2.2. Preparation and in situ reduction of the BC/GO nanocomposite films

The stable aqueous dispersion of GO with a concentration of 0.1 mg/mL was prepared by ultrasonication of powdery GO for 1 h (200 W). 1.0 g dry BC was first swollen in 45 mL of water for 24 h, and then 4.2 g NaOH was added by the assistant of ultrasonication at 0–5 °C. The suspension was cooled to −20 °C and held at that temperature for 6 h. The frozen solid was then allowed to thaw at 5 °C, and 55 mL water was added to the gel-like BC suspension. After stirring for 10 min, a clear BC suspension was obtained. The insoluble part was eliminated by the centrifugation at 1000 rpm for 3 min.

For the preparation of the BC/GO nanocomposite, GO and BC aqueous suspensions were mixed together in several fixed proportions, followed by stirring for 24 h at room temperature. The weight contents of GO in the composites were controlled to be ∼1% and 5%. Before filtration, the BC/GO composite was ultrasonicated for 30 min with a power of 100 W. The homogeneous dispersions were filtered through porous poly(tetrafluoroethylene) membranes (47 mm in diameter and 0.2 μm in pore size) to yield free-standing disc-like films. Finally, the films were dried for 24 h at 50 °C under vacuum. The reduction of GO was carried out by adding 5 μL hydrazine into the BC/GO suspension. The BC/RGO complex was well-dispersed after stirring for 10 h at 80 °C. The preparation of the BC/RGO film was the same to that of BC/GO.

2.3. Characterization

The GO nanosheets were characterized by transmission electron microscope (TEM, Philips Tecnai G2 F20 operating at 200 kV) and atomic force microscope (AFM, Nanoscope MultiMode IIIA). The AFM samples were prepared by depositing a dilute aqueous GO dispersion on a freshly cleaved mica surface. SEM analysis was performed on a Hitachi S-4800 electron microscope (operating at 5 kV). FT-IR spectra were recorded on a Bruker Tensor 27 spectrometer with a disc of KBr. The X-ray diffraction (XRD) patterns were taken by a Rigaku D/max 2500 V/pc X-ray diffractometer using Cu Kα radiation ($\lambda = 0.15$ nm) at a scanning rate of 8.0°/min, using a voltage of 40 kV and a current of 200 mA. Tensile tests of the BC/GO films were performed on a universal tensile testing machine (M350-20KN CX) at a cross-head speed of 0.5 mm/min. Rectangular specimens of 5 mm × 30 mm were used for tensile tests under ambient conditions (with humidity of ∼30%). The film thickness was read from its cross-section SEM image. Five parallel measurements were carried out for each sample and the average value was recorded. The conductivity of the nanocomposite films was measured using a Keithley 2635 system sourcemeter.

3. Results and discussion

3.1. Microscopic analysis of GO

The as-prepared GO is presented almost entirely as individual sheets in the aqueous suspension confirmed by the AFM and TEM measurements. Fig. 1(a) shows the tapping mode AFM image of GO and its corresponding height profiles on a mica substrate. As shown, individual GO sheets with thickness of 0.9–1 nm are observed with lateral dimensions of several hundred nanometers for a fully exfoliated GO sheet. A TEM sample was prepared by dipping a carbon grid into the GO aqueous solution. Wrinkled individual GO sheets in low-magnification image are observed. The individual suspended GO sheets are important for the well dispersion in the BC matrix.

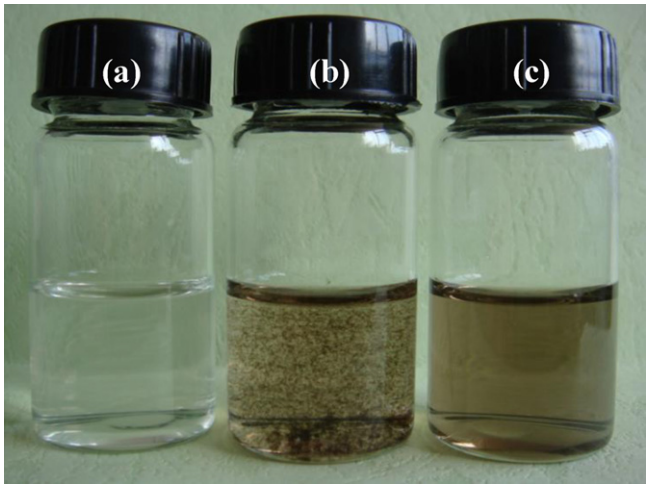

Fig. 2. Solutions of (a) BC, (b) GO, and (c) BC/5 wt% GO in aqueous NaOH.

3.2. Optical observation

The solutions of pure BC, GO and BC/5 wt% GO nanocomposite in aqueous NaOH are shown in Fig. 2. The photograph was taken after 30 min sonication (100 W) and standing for 5 h. As shown in Fig. 2(a), BC forms a homogeneous suspension in aqueous NaOH solution. GO nanosheets tend to aggregate because the inclusion of NaOH destroys the electrostatic repulsion balance of the GO lattices. After 5 h standing, the stable BC/GO suspension indicates that BC can effectively prevent the aggregation of GO at high NaOH concentration. This homogeneous BC/GO suspension is essential to prepare uniform BC/GO composite films.

3.3. SEM observation

The BC/GO flexible paper-like films are obtained by a vacuum-assisted method. Fig. 3 shows the surface and cross-section SEM images of BC, GO, and the BC/GO nanocomposite films with different GO loadings (1 wt% and 5 wt%). The BC sample shows highly fibrous network-like structure consisting of ultrafine cellulose microfibrils (Fig. 3a). The typical lateral dimension of the BC fibrils is 30–40 nm. Its cross-section shows a random arrangement of ribbon-shaped microfibrils without any preferential orientation. Fig. 3c shows the rough surface of the GO film, from which wrinkled GO sheets can be identified. The fracture edge of the film exhibits a compact layer-by-layer stacking structure. After the integration of GO nanosheets, the surfaces of the nanocomposite films form a more compacted morphology and the cross-sections exhibit a layered structure because of the vacuum application and self-ordering of high-aspect ratio GO sheets. Both the surface and cross-section images indicate that the vacuum-assistant method can be used to prepare compacted BC/GO nanocomposite films.

3.4. FT-IR analysis

FT-IR measurements were carried out to investigate the interactions between BC and GO. In the spectrum of GO (Fig. 4a), the broad and intense peak centered at 3361 cm^{-1} is assigned to the O–H stretching vibrations, the strong peak at 1726 cm^{-1} corresponds to the stretching vibrations of C=O carboxylic moieties. The peak at 1616 cm^{-1} is attributed to the skeletal vibrations of aromatic C=C bond or the deformation vibrations of the O–H band of intercalated water molecules (Park, Lee, Bozoklu, Cai, Nguyen, & Ruoff, 2008; Si & Samulski, 2008). In the case of BC, the dominating signal is at 3348 cm^{-1}, corresponding to the intramolecular hydrogen bond for 3O···H–O5 (Oh, Yoo, Shin, & Kim, 2005). In the C–O stretching vibration region, the band at 1163, 1111, 1061 and 1035 cm^{-1} are assigned to the vibrations of C1–O–C4, C2–O2H, C3–O3H and $C6H_2$–O6H, respectively (Kačuráková, Smith, Gidley, & Wilson, 2002; Maréchal & Chanzy, 2000). The peak at 1651 cm^{-1} is attributed to the carbonyl amide group, which may come from proteins and bacterial cells that are not completely wiped off after the NaOH treatment (Shezad, Khan, Khan, & Park, 2010). The characteristic vibrations in the spectra of BC/GO nanocomposites are approximately similar with the spectrum of pure BC as shown in Fig. 4(c) and (d) except for some differences. Compared with pure BC, the C=O stretching vibration peak at 1726 cm^{-1} belonging to GO becomes more evident with the increase of GO loadings in the spectra of the BC/GO composite films, which indicates the existence of GO. The broadened peak at 3348 cm^{-1} and the relative intensity changes of the C–O stretching vibrations in the BC/GO nanocomposites imply the hydrogen bonds in BC are disturbed. Moreover, the peak corresponding to the –CO–NH– stretching vibration shifts to a lower wavenumber (from 1651 to 1643 cm^{-1}). These changes could be ascribed to the strong interaction between BC and GO. It has been proved that the chemical treatment gives rise to a series of oxygen-containing groups on GO sheets such as hydroxyl, epoxyl, and carboxyl groups. Effective interaction such as hydrogen bonding between the oxygen groups on GO and the hydroxyl groups in the BC unit is potentially achievable.

3.5. XRD study

The XRD patterns of the BC/GO films with different GO loadings are shown in Fig. 5. In the case of pure BC, three characteristic peaks centered at 14.8°, 16.7° and 22.7° are observed, corresponding to the typical profile of cellulose I allomorph (Oh et al., 2005; Uhlin, Atalla, & Thompson, 1995). The characteristic 2θ peak of GO appearing at 12.1° corresponds to the (0 0 1) inter-planar spacing of 0.73 nm caused by the oxygen-rich groups on both sides of the sheets and water molecules trapped between the sheets (Bourlinos, Gournis, Petridis, Szabó, Szeri, & Dékány, 2003; Wu et al., 2009). For BC with different GO contents, the peaks of BC become weak but are still observed, while the (0 0 1) peak corresponding to GO is not observed, indicating the GO nanosheets are exfoliated and uniformly dispersed in the BC matrix (Han, Yan, Chen, Li, & Bangal, 2011). The relative crystallinity index is estimated by Segal's method (Segal, Creely, Martin, & Conrad, 1959), using the following equation:

$$C_I = \frac{100[I(0\,0\,2) - I_{am}]}{I(0\,0\,2)}$$

where $I(0\,0\,2)$ is the peak intensity of the (0 0 2) lattice diffraction at $2\theta = 22.7°$ for cellulose I, and I_{am} is the intensity diffraction of amorphous fraction at $2\theta = 18°$. The relative crystallinity index C_I of BC equals 78.7%. After the incorporation of GO nanosheets, the C_I is calculated to be 75.8% for BC with 5 wt% GO loading, which means the GO nanosheets disturbed the aggregation and crystallinity of the BC matrix.

3.6. Tensile test

Mechanical properties of the BC/GO nanocomposite films depend not only on fibril modulus but also on orientation and degree of interaction between BC and GO within the film obtained with the assistance of a vacuum. Fig. 6 illuminates the typical stress–strain curves of pristine BC and its composites with GO, and the mechanical properties of the films are summarized in Table 1. It is clear that both the BC/GO nanocomposites and BC show typical brittle properties and no yielding point can be observed. The Young's modulus and tensile strength of the composite films

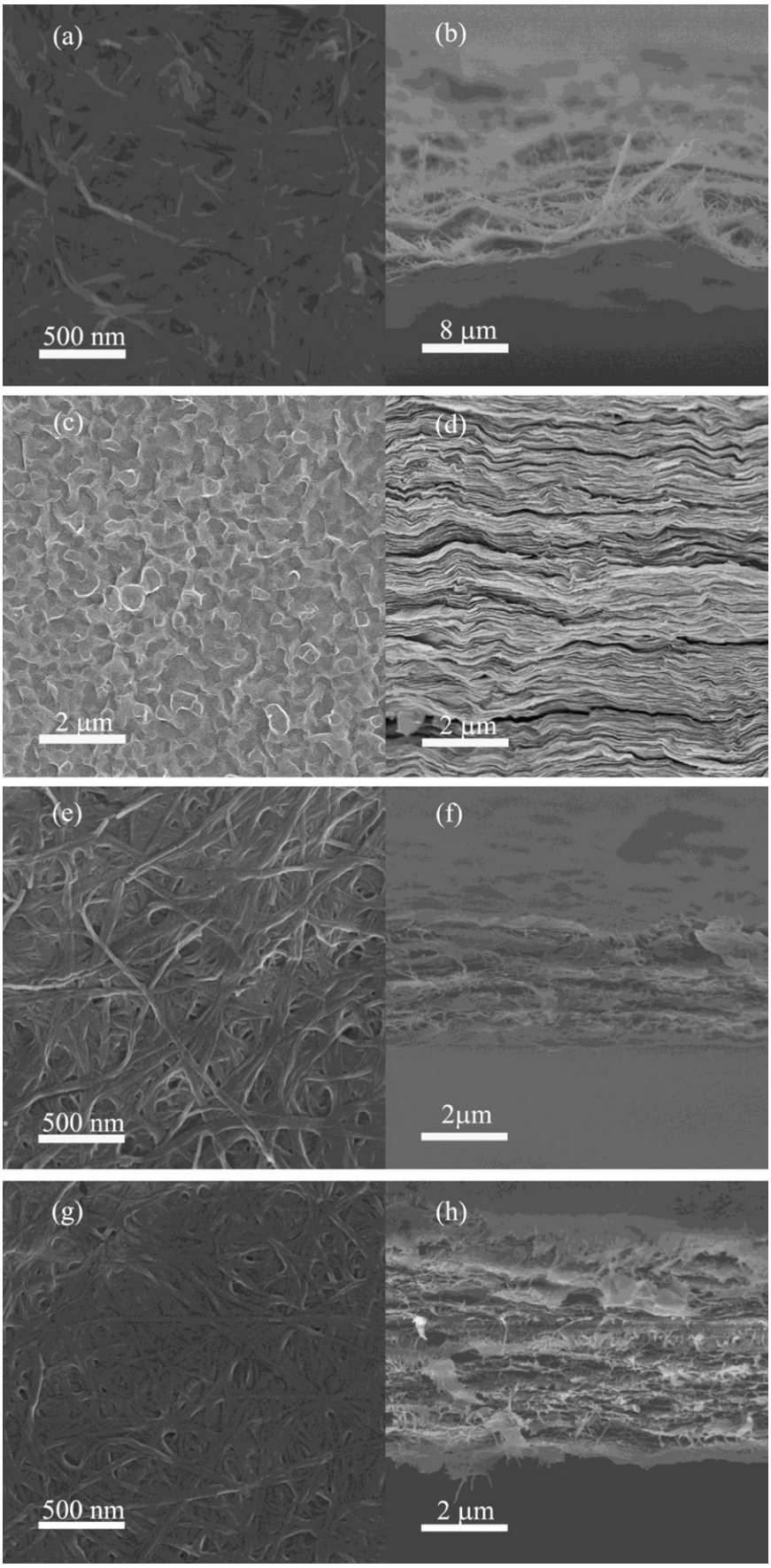

Fig. 3. The surface and cross-section SEM images of BC (a and b), GO (c and d), BC/1 wt% GO (e and f), and BC/5 wt% GO (g and h).

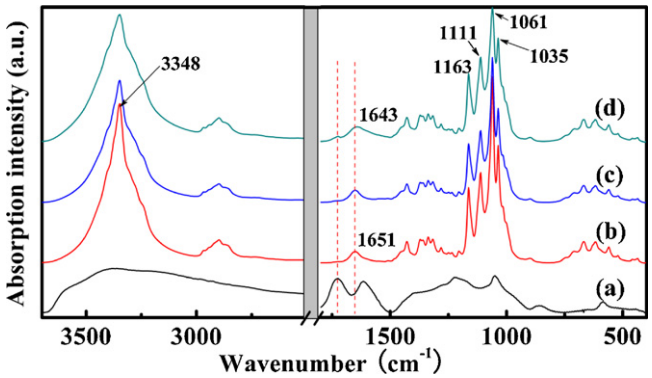

Fig. 4. FT-IR spectra of (a) GO, (b) BC, (c) BC/1 wt% GO, and (d) BC/5 wt% GO.

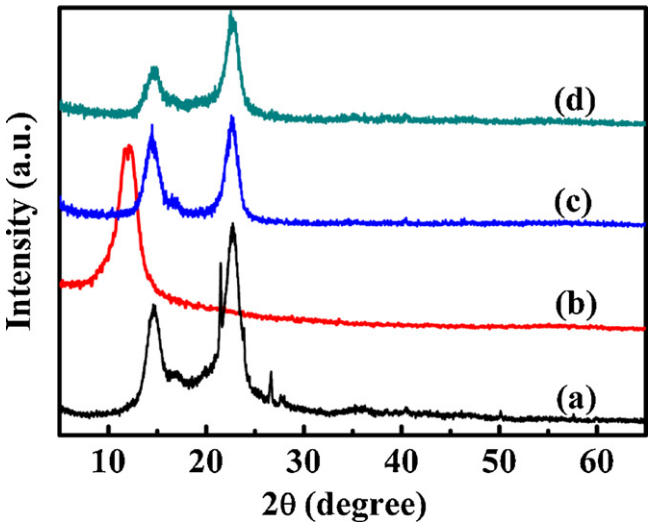

Fig. 5. XRD patterns of (a) BC, (b) GO, (c) BC/1 wt% GO, and (d) BC/5 wt% GO.

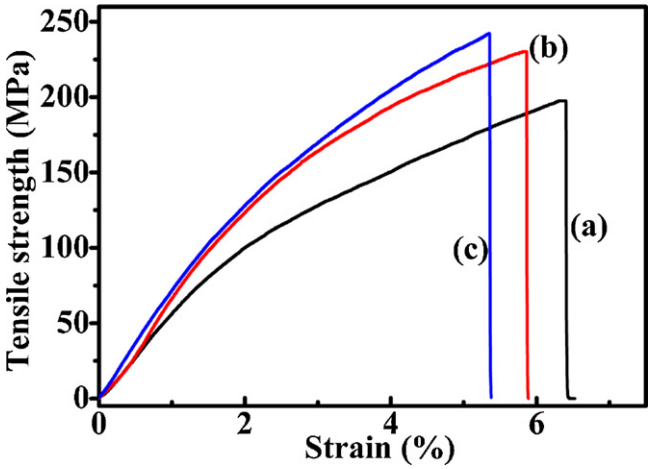

Fig. 6. Typical stress–strain curves of (a) BC, (b) BC/1 wt% GO, and (c) BC/5 wt% GO nanocomposite films.

Table 1
The mechanical properties of BC/GO nanocomposite films with different GO loadings.

Samples	Young's modulus (GPa)	Tensile strength (MPa)	Elongation at break (%)
BC	1.5 ± 0.2	198 ± 10	6.4 ± 0.6
BC/1 wt% GO	1.8 ± 0.2	230 ± 8	5.9 ± 0.6
BC/5 wt% GO	1.7 ± 0.2	242 ± 7	5.4 ± 0.4

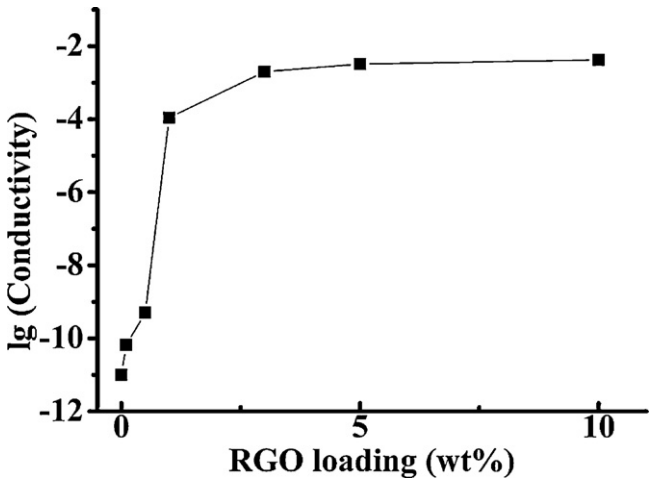

Fig. 7. The conductivity of the BC/RGO nanocomposite films with different RGO weight contents.

enhanced obviously compared with the pristine BC film. For example, the modulus and tensile strength of the BC/GO film with 5 wt% GO are measured to be 1.7 ± 0.2 GPa and 242 ± 7 MPa, respectively. The values are 10% and 20% higher than do BC film, indicating that the interaction between BC and GO makes a great contribution to the mechanical enhancement. As discussed above, the oxygen-containing groups on GO can interact with BC through hydrogen bonding. The high aspect ratio of the GO sheets is also favorable to stress transfer. The unidirectional dispersion of GO nanosheets on the molecular scale in BC matrix and the hydrogen bonding interaction between GO and BC greatly enhance the mechanical properties of the composite films. But the elongation at break decreases from 6.4% (BC) to 5.4% (BC/5 wt% GO) due to the brittle nature of the GO sheets.

3.7. Conductivity measurement

The conductivity of the nanocomposite films with different RGO contents is shown in Fig. 7. After the reduction using hydrazine, the sp^2 structure of GO was partly restored, and the conductivity of the composite films enhanced with the increase of RGO contents. When the RGO content increased from 0.1 wt% to 1 wt%, the conductivity of the film increased by 6 orders of magnitude to 1.1×10^{-4} S/m. The uniformly dispersed RGO improved the conductivity of the BC matrix, probably due to the formation of conductive networks throughout the insulating matrix. With higher RGO contents (>1 wt%), the enhancement of the conductivity is mainly due to its high RGO content. The conductive property of the BC-based nanocomposite films makes it a promising candidate for biosensor and tissue engineering applications.

4. Conclusions

BC/GO nanocomposite films were prepared using a simple vacuum-assisted self-assembly technique. The well-dispersed GO nanosheets in the BC matrix were demonstrated by the SEM and XRD studies. The integration of 5 wt% GO resulted in 10% and 20% increase in Young's modulus and tensile strength of the BC/GO film compared with pristine BC. The interactions between BC and GO such as hydrogen bonding and the unidirectional uniform dispersion of GO nanosheets in BC matrix play important roles in the mechanical improvements. After in situ reduction, the well dispersed RGO sheets form a continuous conductive network throughout the BC matrix, resulting in a remarkable increase by 6 orders of magnitude in the electrical conductivity compared with

the insulated BC. The flexible and electrically conductive BC/GO composite film with desirable mechanical properties is one of promising candidates for advanced biochemical and electrochemical devices.

Acknowledgements

This work was supported by the National Basic Research Program of China (2010CB934700) and the National Natural Science Foundation of China (grant nos. 51173127, 51073115, 51003072, and 51011140072) and the Natural Science Foundation of Tianjin City (no. 10JCZDJC22400).

References

Becerril, H. A., Mao, J., Liu, Z. F., Stoltenberg, R. M., Bao, Z. N., & Chen, Y. S. (2008). Evaluation of solution-processed reduced graphene oxide films as transparent conductors. *ACS Nano*, *2*(3), 463–470.

Bourlinos, A. B., Gournis, D., Petridis, D., Szabó, T., Szeri, A., & Dékány, I. (2003). Graphite oxide: Chemical reduction to graphite and surface modification with primary aliphatic amines and amino acids. *Langmuir*, *19*(15), 6050–6055.

Chen, P., Kim, H. S., Kwon, S. M., Yun, Y. S., & Jin, H. J. (2009). Regenerated bacterial cellulose/multi-walled carbon nanotubes composite fibers prepared by wet-spinning. *Current Applied Physics*, *9*(2), e96–e99.

Czaja, W. K., Young, D. J., Kawecki, M., & Brown, R. M. (2007). The future prospects of microbial cellulose in biomedical applications. *Biomacromolecules*, *8*(1), 1–12.

El-Saied, H., Basta, A. H., & Gobran, R. H. (2004). Research progress in friendly environmental technology for the production of cellulose products (bacterial cellulose and its application). *Polymer—Plastics Technology and Engineering*, *43*(3), 797–820.

Han, D. L., Yan, L. F., Chen, W. F., Li, W., & Bangal, P. R. (2011). Cellulose/graphite oxide composite films with improved mechanical properties over a wide range of temperature. *Carbohydrate Polymers*, *83*(2), 966–972.

Hummers, W. S., & Offeman, R. E. (1958). Preparation of graphitic oxide. *Journal of the American Chemical Society*, *80*, 1339.

Isogai, A., & Atalla, R. H. (1998). Dissolution of cellulose in aqueous NaOH solutions. *Cellulose*, *5*(4), 309–319.

Kačuráková, M., Smith, A. C., Gidley, M. J., & Wilson, R. H. (2002). Molecular interactions in bacterial cellulose composites studied by 1D FT-IR and dynamic 2D FT-IR spectroscopy. *Carbohydrate Research*, *337*, 1145–1153.

Klemm, D., Heublein, B., Fink, H. P., & Bohn, A. (2005). Cellulose: Fascinating biopolymer and sustainable raw material. *Angewandte Chemie-International Edition*, *44*(22), 3358–3393.

Klemm, D., Schumann, D., Udhardt, U., & Marsch, S. (2001). Bacterial synthesized cellulose—artificial blood vessels for microsurgery. *Progress in Polymer Science*, *26*(9), 1561–1603.

Kovtyukhova, N. I., Olliver, P. J., Martin, B. R., Mallouk, T. E., Chizhik, S. A., Buzaneva, E. V., et al. (1999). Layer-by-layer assembly of ultrathin composite films from micron-sized graphite oxide sheets and polycations. *Chemistry Materials*, *11*(3), 771–778.

Maréchal, Y., & Chanzy, H. (2000). The hydrogen bond network in I_β cellulose as observed by infrared spectrometry. *Journal of Molecular Structure*, *523*, 183–196.

Nakagaito, A. N., Iwamoto, S., & Yano, H. (2005). Bacterial cellulose: The ultimate nano-scalar cellulose morphology for the production of high-strength composites. *Applied Physics A: Materials Science and Processing*, *80*(1), 93–97.

Oh, S. Y., Yoo, D. I., Shin, Y., & Kim, H. C. (2005). Crystalline structure analysis of cellulose treated with sodium hydroxide and carbon dioxide by means of X-ray diffraction and FTIR spectroscopy. *Carbohydrate Research*, *340*(15), 2376–2391.

Park, S., Lee, K. S., Bozoklu, G., Cai, W., Nguyen, S. T., & Ruoff, R. S. (2008). Graphene oxide papers modified by divalent ions-enhancing mechanical properties via chemical cross-linking. *ACS Nano*, *2*(3), 572–578.

Park, W. I., Kim, H. S., Kwon, S. M., Hong, Y. H., & Jin, H. J. (2009). Synthesis of bacterial celluloses in multiwalled carbon nanotube-dispersed medium. *Carbohydrate Polymers*, *77*(3), 457–463.

Salavagione, H. J., Gomez, M. A., & Martinez, G. (2009). Polymeric modification of graphene through esterification of graphite oxide and poly(vinyl alcohol). *Macromolecules*, *42*(17), 6331–6334.

Segal, L., Creely, J. J., Martin, A. E., Jr., & Conrad, C. M. (1959). An empirical method for estimating the degree of crystallinity of native cellulose using the X-ray diffractometer. *Textile Research Journal*, *29*(10), 786–794.

Sellinger, A., Weiss, P. M., Nguyen, A., Lu, Y. F., Assink, R. A., Gong, W. L., et al. (1998). Continuous self-assembly of organic–inorganic nanocomposite coatings that mimic nacre. *Nature*, *394*(6690), 256–260.

Shezad, O., Khan, S., Khan, T., & Park, J. K. (2010). Physicochemical and mechanical characterization of bacterial cellulose produced with an excellent productivity in static conditions using a simple fed-batch cultivation strategy. *Carbohydrate Polymers*, *82*, 173–180.

Si, Y. C., & Samulski, E. T. (2008). Synthesis of water soluble graphene. *Nano Letters*, *8*(6), 1679–1682.

Stankovich, S., Piner, R. D., Nguyen, S. T., & Ruoff, R. S. (2006). Synthesis and exfoliation of isocyanate-treated graphene oxide nanoplatelets. *Carbon*, *44*(15), 3342–3347.

Steurer, P., Wissert, R., Thomann, R., & Mulhaupt, R. (2009). Functionalized graphenes and thermoplastic nanocomposites based upon expanded graphite oxide. *Macromolecular Rapid Communications*, *30*(4-5), 316–327.

Uhlin, K. I., Atalla, R. H., & Thompson, N. S. (1995). Influence of hemicelluloses on the aggregation patterns of bacterial cellulose. *Cellulose*, *2*, 129–144.

Vandamme, E. J., De Baets, S., Vanbaelen, A., Joris, K., & De Wulf, P. (1998). Improved production of bacterial cellulose and its application potential. *Polymer Degradation and Stability*, *59*(1–3), 93–99.

Wu, X. L., & Liu, P. (2010). Facile preparation and characterization of graphene nanosheets/polystyrene composites. *Macromolecular Research*, *18*(10), 1008–1012.

Wu, Z. S., Ren, W. C., Gao, L. B., Zhao, J. P., Chen, Z. P., Liu, B. L., et al. (2009). Synthesis of graphene sheets with high electrical conductivity and good thermal stability by hydrogen arc discharge exfoliation. *ACS Nano*, *3*(2), 411–417.

Xu, J. J., Wang, K., Zu, S. Z., Han, B. H., & Wei, Z. X. (2010). Hierarchical nanocomposites of polyaniline nanowire arrays on graphene oxide sheets with synergistic effect for energy storage. *ACS Nano*, *4*(9), 5019–5026.

Yan, Z. Y., Chen, S. Y., Wang, H. P., Wang, B., Wang, C. S., & Jiang, J. M. (2008). Cellulose synthesized by *Acetobacter xylinum* in the presence of multi-walled carbon nanotubes. *Carbohydrate Research*, *343*(1), 73–80.

Yang, J. Z., Sun, D. P., Li, J., Yang, X. J., Yu, J. W., Hao, Q. L., et al. (2009). In situ deposition of platinum nanoparticles on bacterial cellulose membranes and evaluation of PEM fuel cell performance. *Electrochimica Acta*, *54*(26), 6300–6305.

Yano, H., Sugiyama, J., Nakagaito, A. N., Nogi, M., Matsuura, T., Hikita, M., et al. (2005). Optically transparent composites reinforced with networks of bacterial nanofibers. *Advanced Materials*, *17*(2), 153–155.

Yoon, S. H., Jin, H. J., Kook, M. C., & Pyun, Y. R. (2006). Electrically conductive bacterial cellulose by incorporation of carbon nanotubes. *Biomacromolecules*, *7*(4), 1280–1284.